Journal of the Korean Nuclear Society
Volume 36, Number 3, pp.237~247, June, 2004

Evaluation of Tensile Properties of Cast Stainless Steel Using Ball Indentation Test

Jin Weon Kim
Chosun University
375 Seosuk-dong, Dong-gu, Gwangju, 501-759, Korea
jwkim@chosun.ac.kr

(Received January 16, 2004)

Abstract

To investigate the applicability of automated ball indentation (ABI) tests in the evaluation of the tensile properties of cast stainless steel (CSS), ABI tests were performed on four types of unaged CSS and on 316 stainless steel, all of which had a different microstructure and strength. The reliability of ABI test data was analyzed by evaluating the data scattering of the ABI test and by comparing tensile properties obtained from the ABI test and the tensile test. The results show that the degree of scattering of the ABI test data is reasonably acceptable in comparison with that of standard tensile data, when two points data that exhibit out-of-trend are excluded from five to seven points data tested on a specimen. In addition, the scattering decreases slightly as the content of δ-ferrite in CSS increases. Moreover, the ABI test can directly measure the flow parameters of CSS with error bounds of about ± 10 % for the ultimate tensile stress and the strength coefficient, and about ± 15 % for the yield stress and the strain hardening exponent. The accuracy of the ABI test data is independent of the amount of δ-ferrite in the CSS.

Key Words : automated ball indentation, cast stainless steel, tensile properties, δ-ferrite

1. Introduction

Cast stainless steel (CSS) is used for several components in nuclear power plants (NPPs); for example, pump casings, valve bodies, elbows, fittings, and primary coolant pipes. CSS has a duplex microstructure that consists of about 5 to 25 % δ-ferrite in an austenite matrix [1]. The presence of ferrite in castings improves the stress corrosion cracking resistance, the mechanical strength, and the weld ability [1]. However, it can be detrimental in applications of these components at a higher temperature. In a range of 250 to 450 ℃, which includes the NPP operating temperature, long-term exposure induces thermal aging due to the spinodal decomposition of δ-ferrite, thereby causing a loss of ductility and toughness in the CSS [1,2]. Material degradation by thermal aging is therefore a cause of concern for the safe and reliable operation of these nuclear components. Furthermore, the degradation in the ductility and toughness of these components has been considered in the evaluation of life-extension, periodic safety review, and leak-before-break [2-4].

By using destructive standard test techniques that require intensive material to directly measure the mechanical properties, we can accurately assess the aging degradation of materials. In practice, however, it is difficult to obtain bulk material from the in-service components of an NPP. Thus, in a number of studies, an appropriate test technique for assessing the material degradation of the in-service components of an NPP was developed, and several nondestructive and materially non-intensive testing techniques were proposed [5-8].

One of the testing techniques is the automated ball indentation (ABI) technique. Although the ABI technique is nondestructive and materially non-intensive, it directly measures the current and local deformation behavior of materials. In addition, this technique is reportedly reliable for assessing the irradiation hardening of reactor materials, the variation of material properties in the weld region, and the material degradation of gas pipelines [8-11]. In spite of these advantages, however, the ABI test is sensitive to the surface conditions and microstructure of materials because of its small-diameter ball indenter. To use the ABI test to assess the aging degradation of CSS, therefore, it is necessary to systematically investigate the reliability of the ABI test for a type of CSS with a non-homogeneous duplex microstructure.

The objective of this study is to examine the reliability of the ABI test in evaluating the mechanical properties of CSS with a duplex microstructure. In particular, we investigate in detail the effects of the microstructure of the CSS on the reliability of the ABI test data. Therefore, the ABI tests are performed on four types of unaged CSS with different microstructures, and on 316 stainless steel. With these results, the reliability of the ABI test data is analyzed by evaluating the data scattering of the ABI tests and by comparing the flow properties obtained from the ABI tests and conventional tensile tests.

2. Materials and Experimental Procedure

2.1. Materials

The materials with different strengths and microstructures were considered in this experiment. Thus, we selected four types of unaged CSS. These samples comprised CF8A and three samples of CF8M, namely one with a low ferrite content (CF8M_L), one with a middle ferrite content (CF8M_M), and one with a high ferrite content (CF8M_H). Additionally, 316 stainless steel was used to provide a reference for comparing the microstructure of the different types of CSS. The 316 stainless steel has a homogeneous microstructure although the chemical composition is equivalent to the CF8M samples of CSS. For the experiment, all the CSS samples were made as static casting. They were solution heat-treated at 1100℃ and then quenched to reduce and homogenize the carbide and σ-phase in the castings. Table 1 lists their chemical compositions. These compositions were determined on the basis of the chemical

Table 1 Chemical Compositions of Cast Stainless Steels (as designed)

Material		C	Mn	Si	Cr	Ni	Mo	S	P	Co	Fe
CF8M	L	0.04	0.6	0.8	19.5	11.0	2.5	-	-	-	Balance
	M	0.04	0.6	1.0	19.2	9.6	2.25	0.02	0.03	0.1	Balance
	H	0.04	0.6	1.2	20.0	9.0	2.5	0.02	0.03	0.04	Balance
CF8A		0.04	0.6	1.2	20.5	8.5	-	0.02	0.03	0.1	Balance

Table 2 Mechanical Properties of the Tested Materials

Material	ASME Sec.II		Test Data		
	Eng. yield stress, σ_{ey}[MPa]	Eng. tensile stress, σ_{eu}[MPa]	Eng. yield stress, σ_{ey}[MPa]	Eng.tensile stress,σ_{eu}[MPa]	σ_{eu}-σ_{ey}
SS316	205	515	266.1	681.5	415.4
CF8M_L	205	485	249.4	501.1	251.7
CF8M_M			294.1	617.1	323.0
CF8M_H			326.1	597.4	271.3
CF8A	240	530	287.4	615.5	328.1

composition of the CSS used in the primary coolant pipe of NPPs. The amount of δ-ferrite was estimated by Aubery' s equation [12].

Table 2 presents the yield stress and the ultimate tensile stress of the materials obtained from the tensile tests. It also shows the minimum requirements for the mechanical properties of CF8M and CF8A as provided by Section II of the ASME Boiler and Pressure Vessel code[13]. As shown in Table 2, the mechanical properties of all the materials prepared in this study satisfy the requirements of this section of the ASME code.

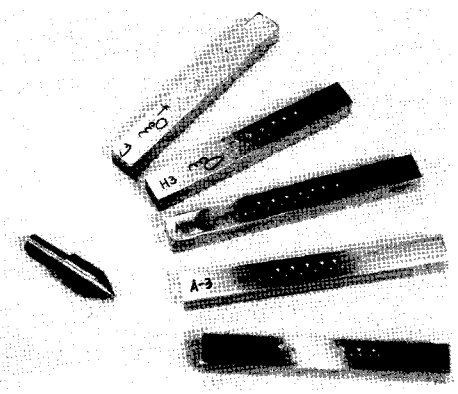

Fig. 1. Specimens Used for the ABI Test

2.2. Specimens and Experimental Procedure

2.2.1. Specimens

In this study, direct comparison of data from the ABI test and a conventional tensile test is important. For the ABI test, therefore, we machined several specimens from each material in the form of a rectangular bar (10 mm × 10 mm × 90 mm or 100 mm), as shown in Fig. 1. These specimens enable us to fabricate a standard tensile specimen after the ABI test. The surfaces of each specimen were machined by milling, and the surface to be indented was polished with #800 emery paper to minimize the effect of surface roughness.

2.2.2. Experimental Procedure

Continuous ball indentation tests were performed in an ABI test system of the Frontics Co. (model ASI-2000 (Fig. 2)). In the ball indentation test, we measured the applied indentation loads and associated penetration depths, and calculated the stress and strain values from these loads and depths using Eqs (1) and (2), which are based on elastic and plastic analyses [14]. These equations are expressed as follows:

$$\sigma = \frac{1}{\Phi}\frac{F}{\pi a^2} \tag{1}$$

$$\varepsilon = \frac{\alpha}{\sqrt{1-(a/R)^2}}\frac{a}{R} \tag{2}$$

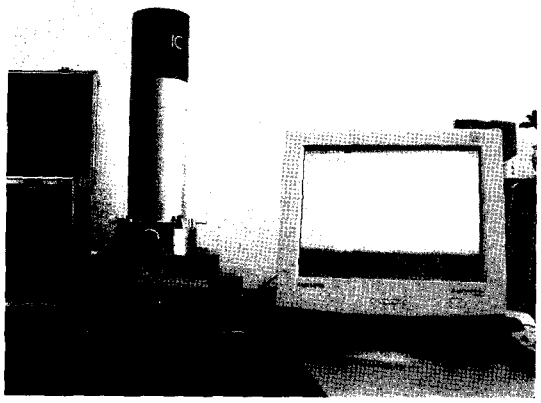

Fig. 2. The ABI Test System Used in Experiment

$$\sigma = K\varepsilon^n \quad (3)$$

where σ is the true stress, ε is the true strain, K is the strength coefficient, n is the strain hardening exponent, a is the indentation radius, R is the ball radius, F is the indentation load, α is a constant, and Φ is the plastic constraint factor [15]. During the indentation, loading and partial unloading are repeated and both stress and strain are calculated at each cycle. Thus, a single indentation gives a flow curve, which is represented by the power law of Eq. (3). By analyzing this curve, we can evaluate the flow parameters of the material involving the yield stress, the ultimate tensile stress, the strength coefficient, and the strain hardening exponent. The software embedded in the ABI test system automatically calculates these factors.

ABI tests were conducted at five to seven points on a surface of each specimen and the results were averaged. To minimize the influence of parameters other than the microstructure of each material, a series of indentation tests was performed along the centerline of each specimen with an equal increment and sufficient space. All tests were carried out at ambient temperature using a tungsten carbide ball indenter of 0.5mm diameter. After the ball indentation tests, three specimens of each material were machined for a standard tensile test; other specimens were aged at 400℃ to simulate the thermal aging of CSS.

3. Results and Discussion

3.1. Microstructure of CSS

To clarify the different microstructures of the CSS specimens, we measured the δ-ferrite content of each specimen using a ferritemeter before the ABI test and observed the morphology of the δ-ferrite using an optical microscope. Table 3 summarizes the mean and standard deviation of the ferrite content for each material. As given in Table 3, the mean values of the δ-ferrite content are 10.1 % for CF8M_L, 20.6 % for CF8M_M, 26.0 % for CF8M_H, and 25.9 % for CF8A, with a standard deviation of less than 1.5 %.

Fig. 3 shows the microstructures of the CSS specimens, in which the size, spacing, and arrangement of the ferrite phase differ with each material. For CF8M_L, which contains about 10% ferrite, the δ-ferrite is independently dispersed in an austenitic matrix with a spacing of about 100μm. For CF8M_M, which contains about 21% ferrite, the δ-ferrite is closely arranged in an austenitic matrix with a spacing of 15 to 20 μm. On the other hand, for CF8M_H, which contains 26 % ferrite, the coarse ferrite phase forms network each other and the spacing is about 50 μm. The CF8A also has a microstructure with a ferrite

Table 3. Content of δ-ferrite for Cast Stainless Steels

Material		Mean [%]	Standard Deviation [%]
CF8M	L	10.1	1.01830
	M	20.6	1.19087
	H	26.0	1.05593
CF8A		25.9	1.54299

network even if the size and spacing are smaller than that of the CF8M_H. These characteristics of the microstructure with the ferrite content support the observations of other studies [2,4,5].

These results indicate that the microstructures of the materials prepared for the experiment have different microstructures as intended, although the ferrite content of CF8M_M and CF8A is higher than expected. By comparing these microstructures with CF8M' s mechanical properties listed in Table 2, we can deduce that the yield stress increases as the content of the δ-ferrite increases, whereas the ultimate tensile stress is higher in CF8M_M than in CF8M_H. This shows that the flow strength of CSS is less dependent on the content of δ-ferrite, although the yield strength is proportional to the δ-ferrite content.

3.2. Reproducibility of the ABI Test Data

To investigate the reproducibility of the ABI test data for CSS, we analyzed the data scattering of the ABI test for each material, using five to seven points of data from the surface of each specimen. The data scattering was quantified by normalizing the standard deviation with the mean value for each parameter. Thus, the mean and standard deviation of the maximum indentation load and flow properties were calculated from the data set of ABI test.

Fig. 4 shows the normalized standard deviations

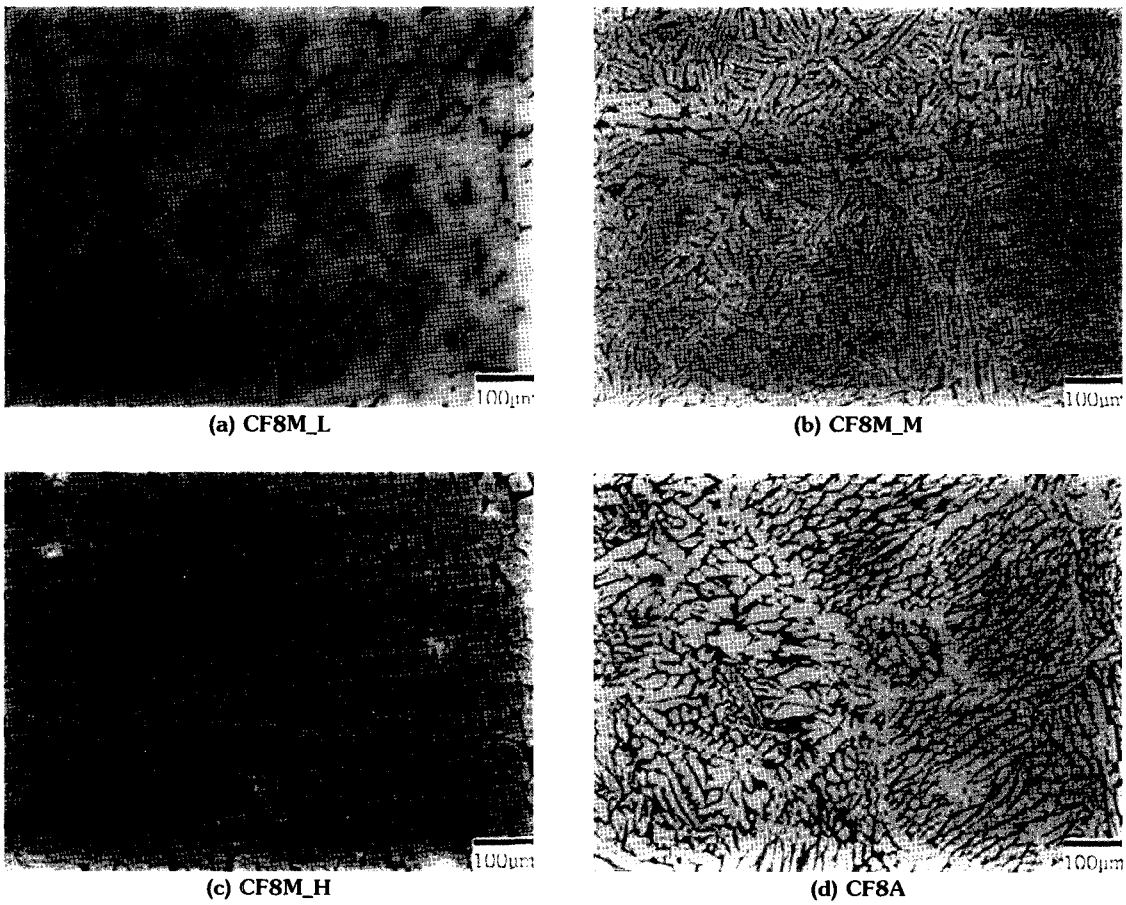

(a) CF8M_L (b) CF8M_M

(c) CF8M_H (d) CF8A

Fig. 3. Microstructures of the Cast Stainless Steels Used in Experiment

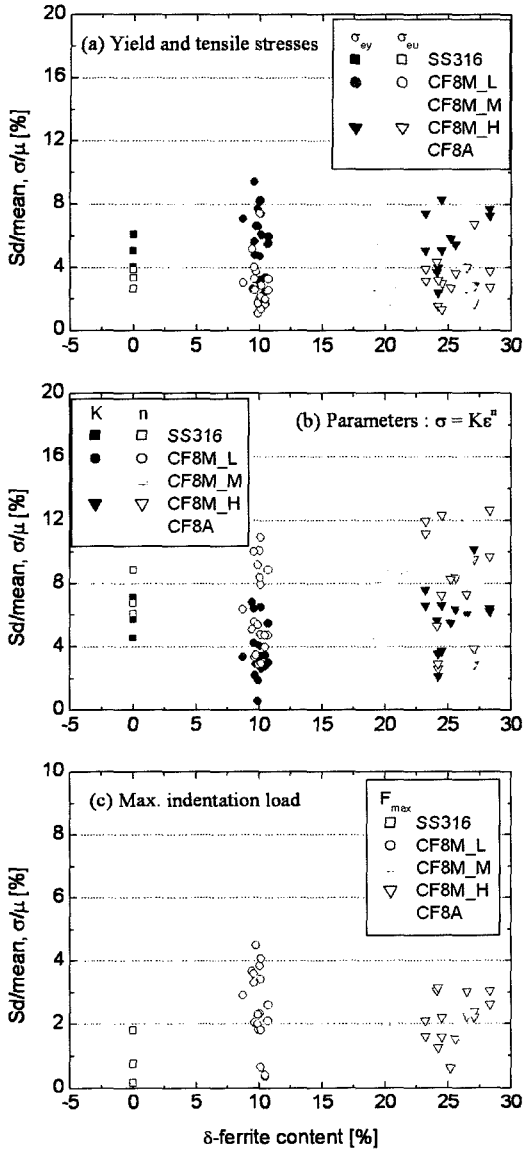

Fig. 4. Normalized Standard Deviations of the Tensile Properties and the Maximum Indentation Load from the ABI Tests, Based on all the Data for Each Specimen

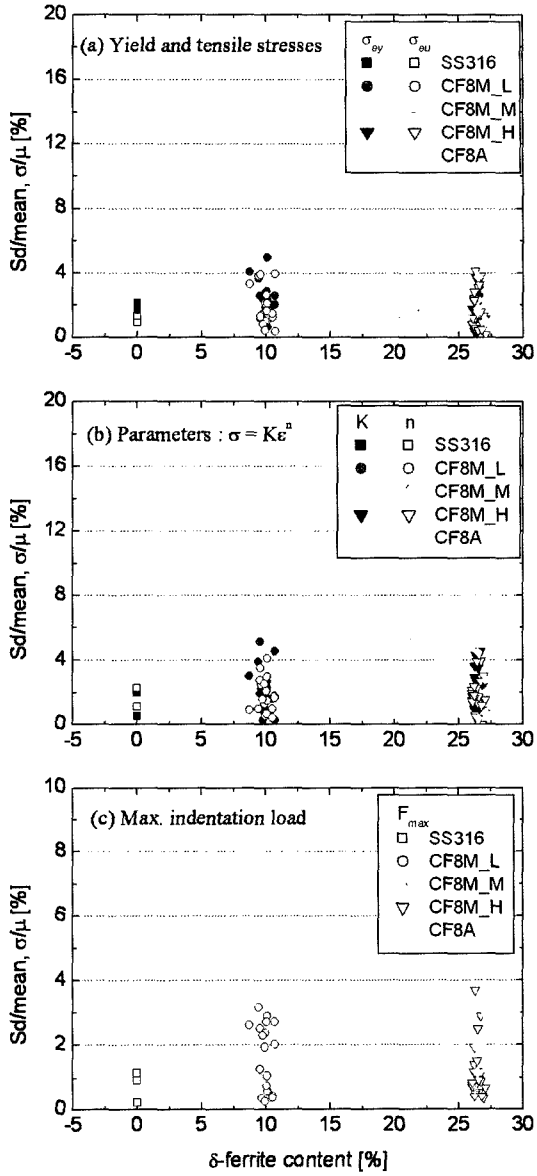

Fig. 5. Normalized Standard Deviations of the Tensile Properties and the Maximum Indentation Load from the ABI Tests, Based on Reduced Data

based on all the data points tested for each specimen as a function of the amount of δ-ferrite. As shown in Fig. 4, the 316 stainless steel with a homogeneous microstructure has the minimum normalized standard deviation for all parameters. For CSS, regardless of the δ-ferrite content, the maximum normalized standard deviation is about 10 % for the yield stress, about 8 % for the tensile

stress, about 10 % for tthe strength coefficient, about 16 % for the strain hardening exponent, and about 5 % for the maximum indentation load. On the other hand, as shown in Fig. 5, when the out-of-trend data of two points are excluded from the all data points, the normalized standard deviations are reduced by about 50 %. The maximum standard deviation is about 5 % for the yield stress and the tensile stress, about 6 % for the strength coefficient and the strain hardening exponent, and about 4 % for the maximum indentation load. Compared with the scattering of the conventional tensile data presented in Fig. 6, this degree of scattering in the ABI test data is reasonably acceptable for the assessment of the tensile

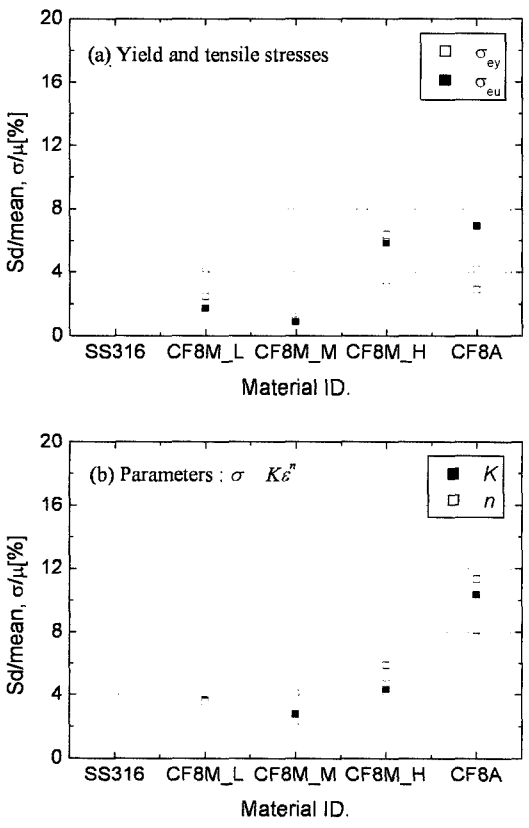

Fig. 6. Normalized Standard Deviations of the Tensile Properties Obtained from the Conventional Tensile Test

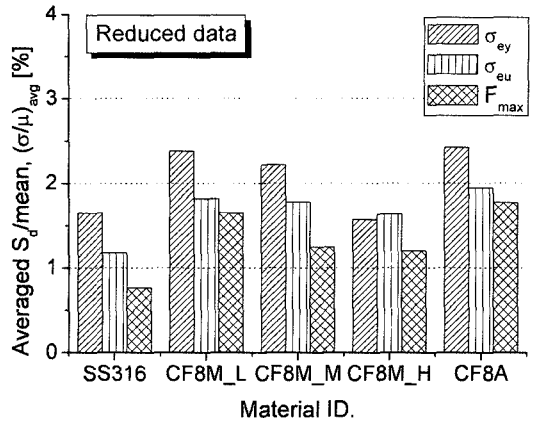

Fig. 7. Comparison of the Averaged Normalized Standard Deviations of the Yield Stress, the Ultimate Tensile Stress, and the Maximum Indentation Load for Each Material

properties of CSS.

In Figs. 4 and 5, the maximum normalized standard deviations are almost the same regardless of the δ-ferrite content. As shown in Fig. 7, however, the averages of the normalized standard deviations are less than 2.5 % for all tested materials, and they decrease slightly as the amount of δ-ferrite in the CF8M increases. This result indicates that the data scattering of the ABI test decreases as the δ-ferrite content in CSS increases. This might be associated with the different morphology of ferrite phase with amount of δ-ferrite in CSS. For the CF8M_L, the δ-ferrite is independently dispersed in an austenitic matrix with large spacing so that the distribution of the stress and strain fields beneath the ball indenter change with the location to be indented. For CSS with higher ferrite content, however, the ferrite phase forms a network; and, as a result, the stress and strain distributions beneath the ball indenter are relatively uniform and less dependent on the indented location.

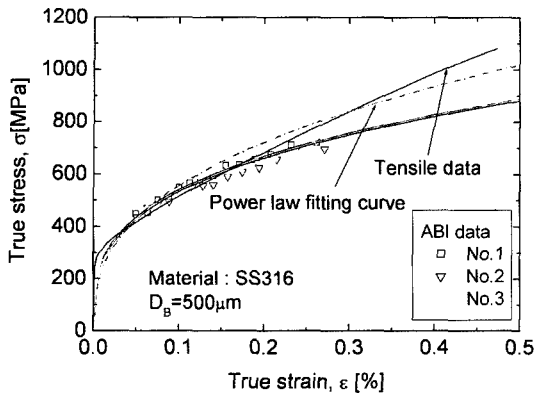

(a) 316 stainless steel

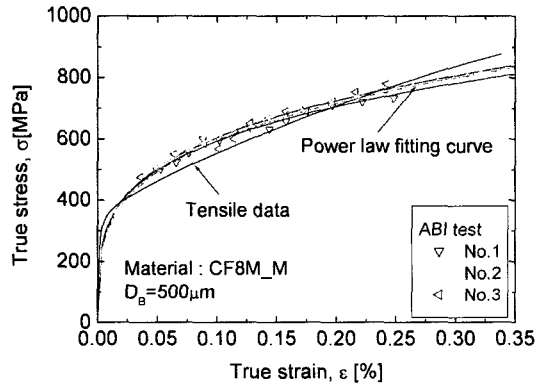

(b) CF8M_M

Fig. 8. Comparison of the Flow Curves Obtained from the ABI Test and the Conventional Tensile Test

3.3. Comparison of Tensile Properties Derived from ABI and Standard Tensile Tests

Fig. 8 compares the stress-strain curves derived from the ABI test with those derived from the conventional tensile test. The flow curves from the ABI test increase parabolically as the strain increases, whereas the curves from the tensile test increase linearly. Thus, the flow stresses from the ABI test are higher than those from the tensile test in a strain range of 3 to 20 % depending on the tested material. This trend is reversed in the other ranges of the strain. This is induced by an inherent characteristic of the ABI model, which assumes that the strain hardening behavior of material complies with the power law of Eq. (3). For stainless steel, however, the strain hardening behavior is almost linear with the strain so that the flow curve is not appropriately represented by the power law adopted in the ABI test. In the results, the stress-strain curves obtained from the tensile test are fitted by Eq. (3), and are compared with those obtained from the ABI test. As shown in Fig. 8(a), the discrepancy in the flow curves is still considerable for the 316 stainless steel, whereas the flow curves of the ABI test agree reasonably well with those of the tensile test for CSS (Fig. 8(b)).

On the other hand, the flow parameters determined from the ABI test were compared with those from a conventional tensile test to quantitatively investigate the accuracy of the ABI test data for CSS. Fig. 9 compares the yield stress, the ultimate tensile stress, the strength coefficient, and the strain hardening exponent from the ABI test with those from the standard tensile test. As shown in Fig. 9(a), the yield stress from the ABI test was in agreement with that of the conventional tensile test where most of the data fell between ± 15 % of the area bounded by the dashed lines. For the ultimate tensile stress, the accuracy was better than for the yield stress, as shown in Fig. 9(b). In this case, except for the 316 stainless steel, the ABI test data agreed with the standard tensile data within ± 10 % of the error bounds. The strength coefficient and the strain hardening exponent also showed a similar agreement where most of the data fell between ± 10 % and ± 15 % of the bounding, respectively.

To examine whether the accuracy of the ABI test results depends on the microstructure of the materials, we averaged the flow parameters and compared them with the standard tensile data for

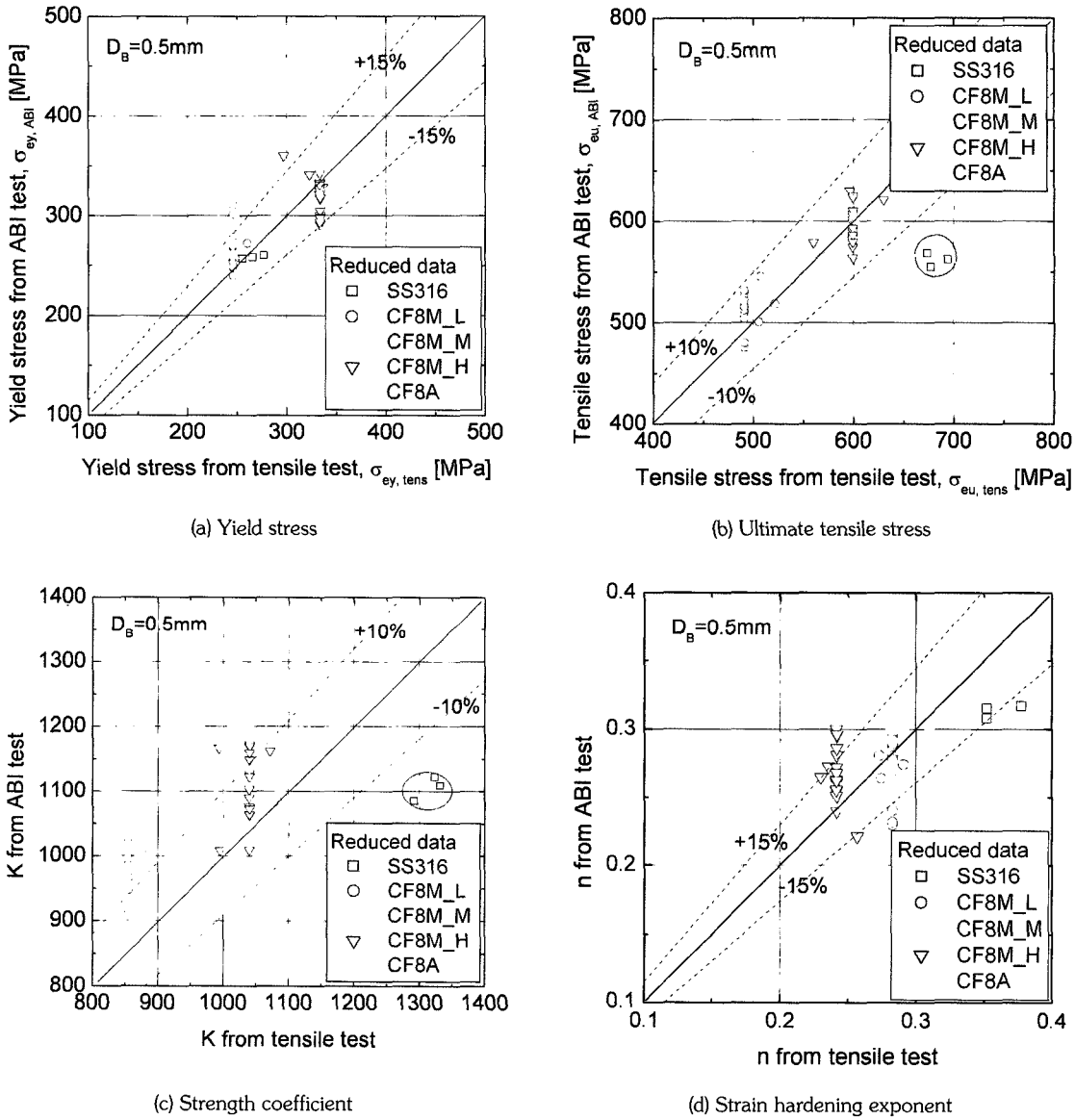

Fig. 9. Comparison of Flow Properties Obtained from ABI and Conventional Tensile Tests

each material. Thus, the error was defined by the difference between the averaged ABI test data and the tensile test data as a normalized form. As shown in Fig. 10, for CSS, the maximum errors were about 9 % for the yield stress, about -7 % for the ultimate tensile stress, and about 12 % for the strength coefficient and the strain hardening exponent. In these results, however, any consistent tendency of error with the type of CSS was not observed for all flow parameters. Moreover, for all flow parameters other than the yield stress, the error was more significant in the 316 stainless steel than in the CSS. Therefore, it is demonstrated that the accuracy of ABI test data

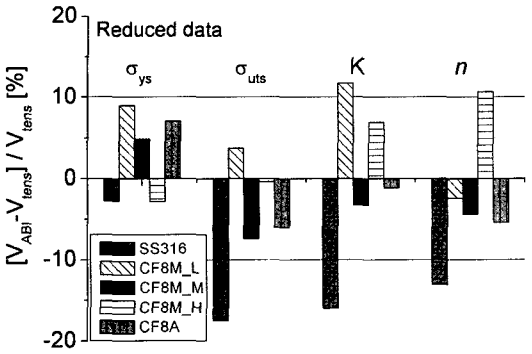

Fig. 10. Comparison of the Relative Errors in the Flow Parameters of the Tested Materials

for CSS is independent on the microstructure of the material, that is, amount of δ-ferrite.

4. Conclusions

To investigate the reliability of the automated ball indentation (ABI) tests in evaluating the mechanical properties of cast stainless steel (CSS), we conducted ABI tests on four unaged CSS and on 316 stainless steel, all of which have a different microstructure and strength. From the results, the following conclusions were obtained:

1) The degree of scattering of the ABI test data is reasonably acceptable compared with that of standard tensile data, when the out-of-trend data of two points are excluded from the data of five to seven points. Moreover, the scattering decreases slightly as the δ-ferrite content in CSS increases.
2) ABI tests appropriately measure the tensile properties of CSS with error bounds of about ± 10 % for the ultimate tensile stress and the strength coefficient, and with about ± 15 % error bounds for the yield stress and the strain hardening exponent. The accuracy of the ABI test data is independent of the amount of δ-ferrite in the CSS.

References

1. D. Peckner and I. M. Bernstein, Handbook of Stainless Steels, p.2-1, McGraw-Hill Book Company, New York (1987).
2. V.N. Shah and P.E. Macdonald, Aging and Life Extension of Major Light Water Reactor Components, p.161, Elsevier Science Pub., Amsterdam(1993).
3. Electric Power Research Institute, "Generic Licence Renewal Technical Issues Summary", EPRI TR-107521, April(1998).
4. O.K. Chopra and W.J. Shack, Assessment of Thermal Embrittlement of Cast Stainless Steel, NUREG/CR-6177, ANL-94/2(1994).
5. T. Goto, T. Naito, and T. Yamaoka, "A study on NDE Method of Thermal Aging of Cast Duplex Stainless Steels", Nucl. Eng. & Des., 182, 181(1998).
6. J.S. Cheon, I.S. Kim, J.G. Jang, J.G. Kim, "Small Punch Test for the Evaluation of Thermal Aging Embrittlement of CF8 Duplex Stainless Steel", Proc. of KNS Spring Meeting(1996).
7. H. Lee and J.H. Lee, "An Indentation Theory Based on FEA Solutions for Property Evaluation", Trans. of KSME (A), 25, 1685(2001).
8. F.M. Haggag, " Effects of Irradiation Temperature on Embrittlement of Nuclear Reactor Vessel Steels", ASTM STP 1175, p.172(1993).
9. F.M. Haggag, " In-situ Nondestructive Measurements of Key Mechanical Properties of Oil and Gas Pipelines", Residual Stress Measurement and General Nondestructive Evaluation, ASME PVP-429, p.99(2001).
10. K.L. Murty, P.Q. Miraglia, M.D. Mathew, V.N. Shah, and F.M. Haggag, "Characterization of Gradients in Mechanical Properties of SA-533B Steel Welds using Ball Indentation", Int.

J. of Pres. Vess. & Piping, 76, 361(1999).

11. T.S. Byun, J.W. Kim, and J.H. Hong, "A Theoretical Model for Determination of Fracture Toughness of Reactor Pressure Vessel Steels in the Transition Region from Automated Ball Indentation Test", J. of Nucl. Mater., 252, 187(1998).
12. L.S. Aubery, P.F. Wieser, W.J. Pollard, and E.A. Schoefer, "Ferrite Measurement and Control in Cast Duplex Stainless Steel", in SS Casting, ASTM STP 756, p.126 ASTM(1982).
13. American Society Mechanical Engineers, ASME Boiler & Pressure Vessel Code, Sec. II, Materials, 1995ed. (1995).
14. Y.H. Lee, J.H. Lee, J.H Ahn, H.S. Park, S.H. Nahm, H.M. Lee, and D. Kwon, "Evaluation of Local Mechanical Properties and Fracture Characteristics Through Indentation Plastic Stress Field", Proc. of the 10th Conf. on Mech. Behaviors of Meter., Ansan, Korea(1996).
15. J.H. Ahn and D. Kwon, "Evaluation of Plastic Flow Properties of Materials through the Analysis of Indentation Load-Depth Curve", J. Kor. Inst. Met. & Mater., 38, 1606(2000).